Low Signal-Attenuation Negative Group-Delay Network Topologies Using Coupled Lines

Girdhari Chaudhary, *Member, IEEE*, and Yongchae Jeong, *Senior Member, IEEE*

***Abstract*—This paper presents the design and analysis of novel topologies of reflective-type negative-group-delay (NGD) networks with very small signal attenuation (SA). The proposed topologies are based on short-circuited coupled lines. Theoretical analysis shows that predefined group-delay (GD) time with very small SA can be obtained due to the high characteristic impedance of a coupled line and the small coupling coefficient. Due to the very low SA characteristics of the proposed networks, the burden of compensating general-purpose gain amplifiers can be reduced and provide stable operations while integrated to RF systems. This paper also analyses performance degradation of the GD time and SA of the proposed NGD networks according to the temperature-dependent resistance variation. For an experimental validation of the proposed topologies, distributed microstrip line NGD networks (type-I and type-II) are designed, simulated, and measured for a wideband code division multiple access (WCDMA) downlink frequency operating at a center frequency of 2.14 GHz. These results show a GD time of −7.27 ns with an SA of 7.43 dB for the type-I NGD network, and −6.3 and 9.23 dB for the type II-NGD network at the center frequency, and agree closely with the simulations. To enhance the NGD bandwidth, two NGD networks with slightly different center frequencies are connected in parallel, which provides wider bandwidth than the single stage case and shows practical applicability.**

***Index Terms*—Coupled lines, distributed transmission line, high characteristic impedance, low signal attenuation (SA), wideband code division multiple access (WCDMA).**

I. Introduction

In RECENT years, there has been an increasing amount of research on negative-group-delay (NGD) networks at microwave frequencies. In a medium of refractive index $n(\omega)$, the dispersion relation [1] can be written as follows:

$$k = \frac{\omega n}{c} \tag{1}$$

where ω, k, and c is angular frequency, wavenumber, and speed of light. The group velocity (v_g) known as the speed of the envelope signal [1] can be given as follows:

$$v_g = \frac{c}{n + \omega \mathrm{Re}(\frac{dn}{d\omega})}. \tag{2}$$

Manuscript received February 09, 2014; revised May 13, 2014 and June 26, 2014; accepted July 04, 2014. Date of publication August 15, 2014; date of current version October 02, 2014. This work was supported by the Basic Science Research Program through the National Research Foundation of Korea (NRF) funded by the Ministry of Education, Science, and Technology (2013006660).

The authors are with the Division of Electronics Engineering, Information Technology Convergence Research Center, Chonbuk National University, Jollabuk-do 561-756, Korea (e-mail: ycjeong@jbnu.ac.kr).

Color versions of one or more of the figures in this paper are available online at http://ieeexplore.ieee.org.

Digital Object Identifier 10.1109/TMTT.2014.2345352

From (1) and (2), it is inferred that if the refractive index n and its derivative with respect to ω are negative (i.e., $dn/d\omega < 0$), the group velocity, and consequently, the group delay (GD), can become negative. This does happens near the absorption line or in media with a signal attenuation (SA) where an "anomalous" wave propagation effect can occur [1], [2]. Typically, the NGD phenomena in RF circuits can be observed within the limited frequency band through the SA condition.

The physical phenomenon referred to as NGD implies a negative delay (i.e., a time advancement). These interesting characteristics of NGD networks have been applied to various practical applications in communication systems, such as shortening or reducing delay lines, enhancing efficiency of a feedforward linear amplifier, enhancing the bandwidth of a feedback linear amplifier, and minimizing beam-squint in phased-array antenna systems [3]–[8]. Recently, new and interesting applications of NGD networks have been reported in the realization of non-Foster reactive elements such as negative capacitances or inductances [9]. They have opened doors for new application fields of NGD networks, such as increasing the capacitance tuning range in a varactor diode [10], or enhancing the efficiency of a class-E power amplifier by using negative capacitance to compensate for the stray capacitance of a transistor [11]. It can also be extended to electromagnetic applications such as increasing the bandwidth of an artificial magnetic conductor by loading with NGD networks as non-Foster elements [12].

Various approaches have been applied to design active/passive microwave NGD networks using *RLC* resonators [13]–[26]. To overcome the limited availability problem of lumped elements in RF and microwave, the NGD networks using distributed elements are also presented in the literature [3], [13], [14], [19], [21]. The major drawback of previously presented NGD networks is their inherent SA; this can be resolved by a gain compensation amplifier at the expense of increased noise due to out-of-band gain and other tradeoffs (such as stability problems).

A few works have been performed regarding NGD networks with small SA. In [26], a composite NGD network with smaller SA is presented. However, this circuit requires parallel lumped elements (such as capacitors and inductors) between two transmission lines, making implementation difficult at microwave frequencies. The distributed-line NGD network with improved SA is presented in [27] and [28]. However, it is also difficult to further improve the SA in [27] because of the difficulty in realizing a transmission line with characteristic impedance above 140 Ω in printed circuit board (PCB) technology [27]. Moreover, the NGD requires two transmission-line resonators (one

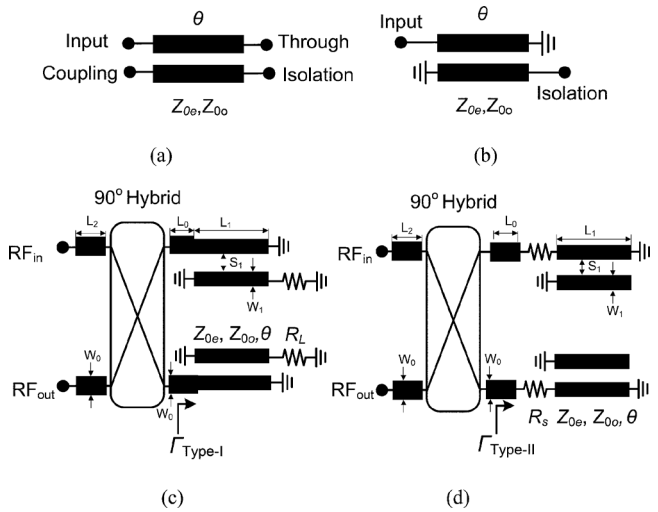

Fig. 1. Structure of NGD networks using coupled lines. (a) Four-port coupled line. (b) Two-port short-circuited coupled line. (c) NGD network type I. (d) NGD network type II.

high characteristic impedance-line resonator and other low characteristic impedance-line resonator), which increase the circuit size.

The reflection-type networks are widely used to design microwave circuits [3], [4], [15], [16], [29]–[31]. Therefore, this paper presents distributed transmission-line reflective-type configuration NGD networks topologies with a predefined NGD time and very low SA. The newly proposed topologies are based on short-circuited coupled lines. Theoretical analysis shows that the GD time and SA are functions of characteristic impedance, the coupling coefficient of the coupled lines and resistor value. The very low SA in the proposed structures can be found due to the high characteristics impedance of coupled lines and weak coupling.

This paper is organized as follows. First, Section II discusses the theory and design equations of low-loss reflective-type NGD (type-I and type-II) networks followed by the performance degradation. Section III describes the simulation and measurement results, and Section IV offers a conclusion.

II. Theory and Design Equations

Fig. 1(a) shows the general structure of a four-port coupled line circuit where odd- and even-mode impedance and electrical length are given as Z_{0o}, Z_{0e}, and θ, respectively. By terminating coupling and through ports in shorts, the coupled line is reduced to a two-port line, as shown in Fig. 1(b). Therefore, admittance parameters (Y-parameters) of the short-circuited two-port coupled line are given as shown in (3) by assuming transverse electromagnetic wave propagation and symmetrical transmission lines [32]

$$[Y] = \begin{bmatrix} -j\frac{Y_{0o}+Y_{0e}}{2}\cot\theta & -j\frac{Y_{0o}-Y_{0e}}{2}\csc\theta \\ -j\frac{Y_{0o}-Y_{0e}}{2}\csc\theta & -j\frac{Y_{0o}+Y_{0e}}{2}\cot\theta \end{bmatrix}. \tag{3}$$

Furthermore, when an isolation port is terminated with a load $Z_L = 1/Y_L$, the input impedance of the coupled line is given as follows:

$$Z_{\text{in}} = \frac{1}{Y_{\text{in}}} = \left[Y_{11} - \frac{Y_{12}Y_{21}}{Y_{22}+Y_L}\right]^{-1}. \tag{4}$$

A. Type-I: Short-Circuited Coupled Line With Resistor Terminated Isolation Port

Fig. 1(c) shows structure of a reflective type-I NGD network, which consists of a 90° 3-dB hybrid coupler, and coupled lines with an isolation port terminated with load $Z_L = R_L$. Since the structure is a reflective type, the transmission coefficient of the proposed NGD network is the same as the input voltage reflection coefficient (Γ_L) at the input port of the coupled line by assuming an ideal and a lossless hybrid coupler. Expressing the effective length of a coupled line as $\theta = \pi f/2f_0$, the input voltage reflection coefficient with port impedance $Z_0 = 1/Y_0$ is given as shown in (5), where f and f_0 are operating and design center frequency, respectively,

$$\left|\Gamma_{\text{Type-I}}\right| \angle\varphi_{\text{Type-I}} = \left|\frac{X_1+X_2}{X_3+X_4}\right| \angle\left(\tan^{-1}\frac{X_2}{X_1} + \tan^{-1}\frac{X_4}{X_3}\right) \tag{5}$$

where

$$X_1 = Z_c^2 C - C^2 R_L Z_0 \csc^2\left(\frac{\pi f}{2f_0}\right) + R_L Z_0 \cot^2\left(\frac{\pi f}{2f_0}\right) \tag{6a}$$

$$X_2 = Z_c C (Z_0 - R_L)\cot\left(\frac{\pi f}{2f_0}\right) \tag{6b}$$

$$X_3 = Z_c^2 C^2 + C^2 R_L Z_0 \csc^2\left(\frac{\pi f}{2f_0}\right) - R_L Z_0 \cot^2\left(\frac{\pi f}{2f_0}\right) \tag{6c}$$

$$X_4 = Z_c C\,(Z_0 + R_L)\cot\left(\frac{\pi f}{2f_0}\right). \tag{6d}$$

Furthermore, the characteristic impedance Z_c, and coupling coefficient C of the coupled line [32], [33] are given as follows:

$$Z_c = \frac{2Z_{0e}Z_{0o}}{Z_{0e}-Z_{0o}} = Z_{0e}\frac{1-C}{C} = Z_{0o}\frac{1+C}{C} \tag{7a}$$

$$C = \frac{Z_{0e}-Z_{0o}}{Z_{0e}+Z_{0o}} \tag{7b}$$

where $Z_{0\text{e}} = 1/Y_{0\text{e}}$ and $Z_{0\text{o}} = 1/Y_{0\text{o}}$ are even- and odd-mode impedances. Therefore, the GD expression of the proposed network is given as follows:

$$\tau_{\text{Type-I}} = -\frac{d\varphi_{\text{Type-I}}}{d\omega} = \frac{X_2X_1' - X_1X_2'}{X_1^2+X_2^2} + \frac{X_4X_3' - X_3X_4'}{X_3^2+X_4^2} \tag{8}$$

where

$$X_1' = \frac{R_L Z_0}{2f_0}(C^2-1)\csc^2\left(\frac{\pi f}{f_0}\right)\cot\left(\frac{\pi f}{f_0}\right) \tag{9a}$$

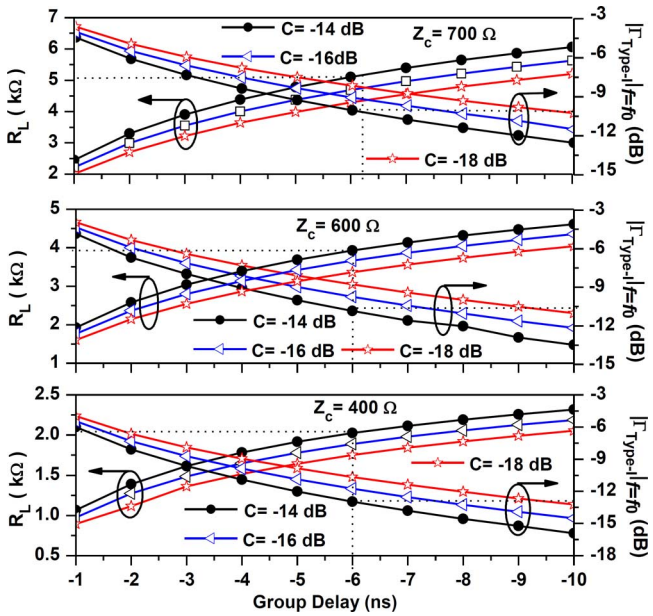

Fig. 2. Calculated maximum achievable GD and magnitude at $f_0 = 2.14$ GHz of the type-I NGD network for different values of Z_c, C, and R_L.

$$X_2' = -\frac{Z_c C}{2f_0}(Z_0 - R_L)\csc^2\left(\frac{\pi f}{f_0}\right) \tag{9b}$$

$$X_3' = -\frac{R_L Z_0}{2f_0}(C^2 - 1)\csc^2\left(\frac{\pi f}{f_0}\right)\cot\left(\frac{\pi f}{f_0}\right) \tag{9c}$$

$$X_4' = -\frac{Z_c C}{2f_0}(Z_0 + R_L)\csc^2\left(\frac{\pi f}{f_0}\right). \tag{9d}$$

Therefore, the maximum achievable GD time and SA can be calculated at $f = f_0$ and are given as follows:

$$\mathrm{SA}_{\text{Type-I}}\Big|_{f=f_0} = \Big|\Gamma_{\text{Type-I}}\Big|_{f=f_0} = \left|\frac{Z_c^2 - Z_0 R_L}{Z_c^2 + Z_0 R_L}\right| \tag{10a}$$

$$\tau_{\text{Type-I}}\Big|_{f=f_0} = -\frac{Z_c Z_0\left(R_L^2 - Z_c^2\right)}{2f_0 C\left(Z_c^4 - R_L^2 Z_0^2\right)}. \tag{10b}$$

From (10a), the maximum SA is a function of Z_c and R_L. As the value of Z_c increases, the SA can be improved. Similarly, the maximum achievable GD time depends on Z_c, R_L, and C, which provide three degrees of freedom to control GD time. For design graph, the calculated maximum achievable GD and SA are plotted in Fig. 2 for different values of Z_c, C, and R_L. As shown in these graphs, for the same GD, the SA can be improved by controlling the C of the coupled lines for the same GD, therefore small C is preferable for a low value of the SA.

Fig. 3 shows the calculated GD and magnitude characteristics of a type-I structure fixed maximum achievable GD of -6 ns. In this structure, the value of Z_c is 600 Ω and C varies from -14 to -18 dB. These figures show that, as the value of C decreases, the SA characteristics improve. However, the NGD bandwidth of the proposed structure becomes narrow, which is defined as bandwidth (NGD BW $= f_2 - f_1$) of 0-ns GD time, as shown in Fig. 3 for convenience. Therefore, there is a tradeoff between GD time, SA characteristics, and the NGD bandwidth.

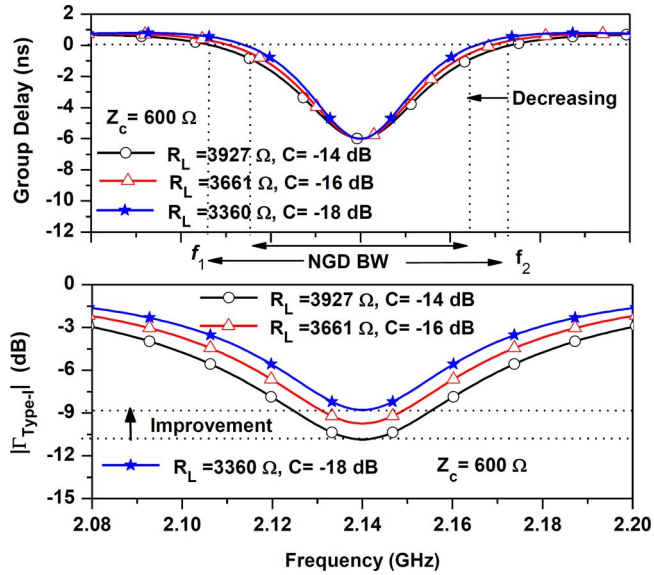

Fig. 3. Calculated GD and magnitude characteristics of the type-I NGD network for different values of C and R_L.

B. Type-II: Short-Circuited Coupled Line With Open-Circuited Isolation Port and Series Connected Resistor at Input Port

Fig. 1(d) shows the structure of a reflective type-II NGD network, which consists of a 90° 3-dB hybrid coupler, series- connected resistor (R_s) at the input port, and short-circuited coupled lines with an open-circuited isolation port and series connected resistor (R_s) at the input port. As described previously, the input voltage reflection coefficient (Γ_S) of this circuit with port impedance $Z_0 = 1/Y_0$ is given as follows in (11) by expressing the effective length of the coupled line as $\theta = \pi f/2f_0$ and by using (4):

$$\begin{aligned}\left|\Gamma_{\text{Type-II}}\right| \angle\varphi_{\text{Type-II}} &= \left|\frac{X_5 + jX_6}{X_7 + jX_8}\right| \angle\left(\tan^{-1}\frac{X_5}{X_6} - \tan^{-1}\frac{X_7}{X_8}\right)\end{aligned} \tag{11}$$

where

$$X_5 = 2(R_s - Z_0)\left(\cos^2\left(\frac{\pi f}{2f_0}\right) - C^2\right) \tag{12a}$$

$$X_6 = X_8 = Z_c C \sin\left(\frac{\pi f}{f_0}\right) \tag{12b}$$

$$X_7 = 2(R_s + Z_0)\left(\cos^2\left(\frac{\pi f}{2f_0}\right) - C^2\right). \tag{12c}$$

Furthermore, the characteristic impedance Z_c and coupling coefficient C of the coupled line are given as (7). The GD expression of this proposed network is given as follows in (13):

$$\begin{aligned}\tau_{\text{Type-II}} &= -\frac{d\varphi_{\text{Type-II}}}{d\omega} \\ &= \frac{X_5 X_6' - X_6 X_5'}{X_5^2 + X_6^2} + \frac{X_7 X_8' - X_8 X_7'}{X_7^2 + X_8^2}\end{aligned} \tag{13}$$

where

$$X_5' = -\frac{(R_s - Z_0)}{2f_0}\sin\left(\frac{\pi f}{f_0}\right) \tag{14a}$$

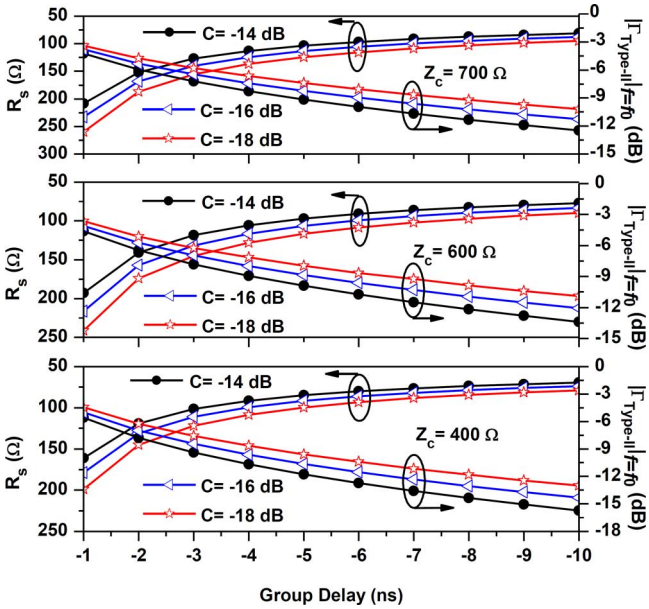

Fig. 4. Calculated maximum achievable GD and magnitude at $f_0 = 2.14$ GHz of the type-II NGD network for different values of Z_c, C, and R_s.

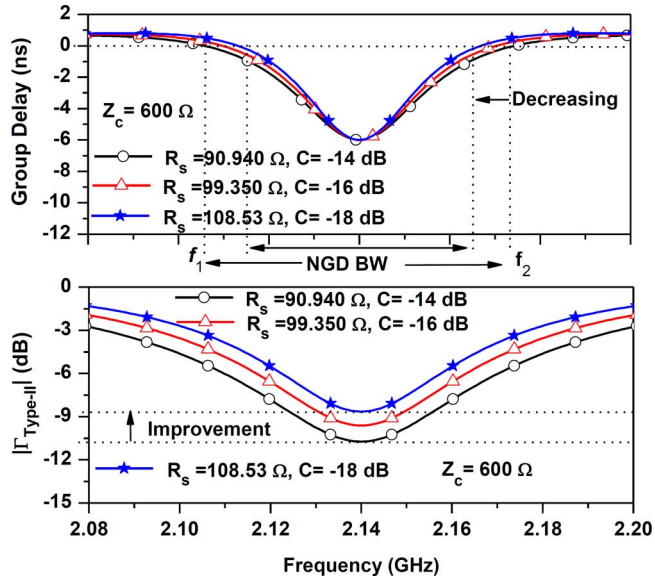

Fig. 5. Calculated GD and magnitude characteristics of the type-II NGD network for different values of C and R_s.

$$X_6' = X_8' = \frac{Z_c C}{2f_0}\cos\left(\frac{\pi f}{f_0}\right) \tag{14b}$$

$$X_7' = -\frac{(R_s + Z_0)}{2f_0}\sin\left(\frac{\pi f}{f_0}\right). \tag{14c}$$

Therefore, the maximum achievable GD time and SA can be calculated at f_0 and are given as follows in (15):

$$\mathrm{SA}_{\text{Type-II}}\Big|_{f=f_0} = \left|\Gamma_{\text{Type-II}}\right|_{f=f_0} = \left|\frac{R_s - Z_0}{R_s + Z_0}\right| \tag{15a}$$

$$\tau_{\text{Type-II}}\Big|_{f=f_0} = -\frac{Z_c Z_0}{2f_0 C\left(R_s^2 - Z_0^2\right)} \tag{15b}$$

where Z_0 is port impedance. As seen from these expressions, the maximum SA is a function of R_s. As R_s increases, the maximum SA can be improved at f_0. Similarly, maximum achievable GD depends on Z_c, C, and $R_s > Z_0$. For a better understanding of (15), the maximum achievable GD and SA are plotted in Fig. 4 according to different values of Z_c, C, and R_s. As shown in these figures, the maximum achievable GD time increase as R_s decreases for fixed values of Z_c and C. Moreover, the SA is improved for small values of C.

Fig. 5 shows the calculated GD and magnitude characteristics of the type-II structure. In this simulation, the maximum achievable GD is fixed as -6 ns. For this purpose, the value of Z_c is 600 Ω, and C is varied from -14 to -18 dB. As shown in these figures, the SA characteristics improve as C decreased. However, the NGD bandwidth of the proposed structure narrows, as shown in Fig. 5. Therefore, there is a tradeoff between GD time, SA characteristics, and the NGD bandwidth.

C. Performance Degradation Analysis

The temperature dependence of a resistor is represented by the following relationship:

$$\frac{\Delta R}{R_0} = \delta \Delta T \tag{16}$$

where δ, R_0, ΔR, and ΔT are the temperature coefficient, initial resistance, resistance variation, and temperature variation, respectively.

Fig. 6 shows the performance degradation of the proposed NGD networks (type-I and type-II) assuming the resistance variation of $\pm 5\%$. As shown in these figures, the GD time and SA variations are approximately ± 1.57 ns and ± 1.0 dB from the reference values for the type-I NGD network, respectively. Similarly, the GD time and SA variations are approximately ± 1.52 ns and ± 0.98 dB from the reference values for the type-II NGD network, respectively. These results indicate that the proposed NGD networks are considerably less sensitive to temperature-dependent resistance variations.

III. Implementation and Experimental Performance

The design method of the proposed NGD networks is summarized as follows.

1) Specify center frequency f_0, maximum achievable GD, and SA.
2) Calculated value of R, Z_c, and C for given value of the SA, GD using (10) for type-I NGD network and using (15) for type-II NGD network.
3) Calculate Z_{0e} and Z_{0o} using (7a) and obtain width, length, and spacing of coupled line according to substrate information.
4) Convert one-port network to two-port network using coupler and optimize the physical dimensions.

To verify the design concept of the proposed structures, two NGD networks (single stage and cascaded stage) are designed and fabricated for the wideband code division multiple access (WCDMA) downlink center frequency (f_0) of 2.14 GHz. The goal was to achieve GD time of -7 ns at f_0 with minimum SA. The circuit is fabricated on a substrate RT/Duroid 5880 from Rogers Inc. with a dielectric constant (ε_r) of 2.2 and a thickness (h) of 31 mil. For the 3-dB hybrid coupler, a quadrature surface mount hybrid coupler S03A2500N1 from Anaren was

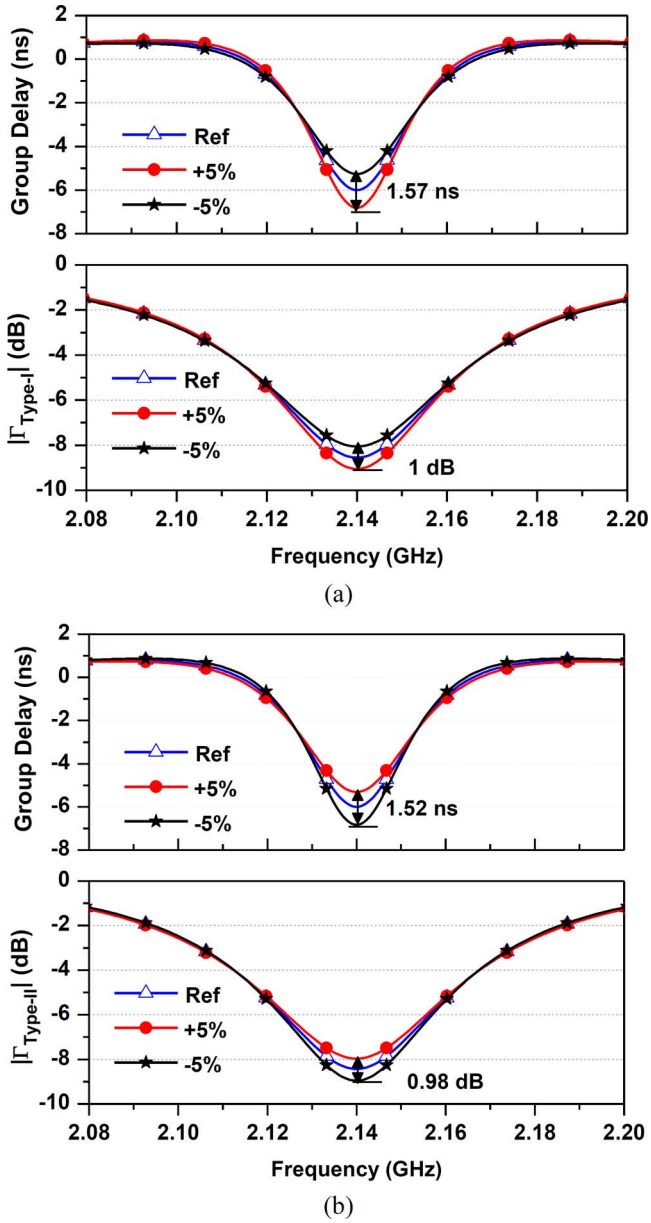

Fig. 6. Performance degradation characteristics of type-I and type-II NGD networks with $Z_{0e} = 90\ \Omega$ and $Z_{0o} = 70\ \Omega$ assuming $\pm 5\%$ variation from the reference value. (a) Type-I and (b) type-II. Ref. value means value at room temperature.

TABLE I
PHYSICAL DIMENSIONS OF SINGLE STAGE TYPE-I AND TYPE-II NGD NETWORKS. (UNITS: MILLIMETERS, REFER TO FIG. 1)

W_0	L_0	W_1	L_1	S_1	L_2	R_L (Ω)	R_s (Ω)
2.40	3	1.04	24.95	1.06	10	3800	105

used for compact circuit size. The simulation is performed using Ansoft's HFSS v13. In order to meet the defined goal, the circuit elements of NGD networks (type-I and type-II) are chosen as $Z_c = 630\ \Omega$, $C = -18.06$ dB, $Z_{0e} = 90\ \Omega$, and $Z_{0o} = 70\ \Omega$. The values of R_L and R_s for type-I and type-II NGD networks are given as 3800 and 105 Ω, respectively. The physical dimensions of these networks after optimization are given in Table I.

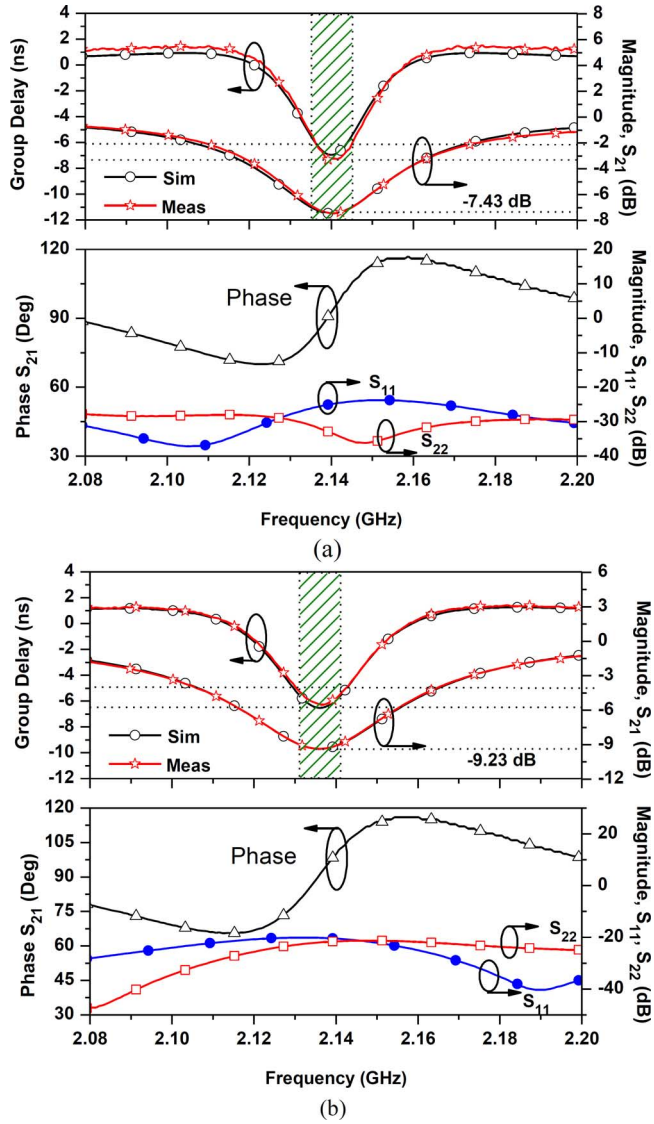

Fig. 7. Simulation and measurement results of single-stage NGD networks. (a) Type-I and (b) type-II.

A. Single-Stage NGD Networks

Fig. 7(a) shows the simulation and measurement results of a type-I single-stage NGD network. As shown in the figure, the measurement results agree with those of the simulation. From the measurement, the maximum achievable GD time of -7.27 ns and an SA of -7.43 dB are obtained at 2.14 GHz. The measured input and output return losses (S_{11} and S_{22}) characteristics are better than 20 dB. As seen from Fig. 7(a), the measured phase slope of S_{21} increases over a certain frequency range.

Fig. 7(b) shows the performance of the type-II single-stage NGD network. As show in the figure, the measurement results agree with those of the simulation. From the measurement, the maximum achievable GD time of -6.30 ns and SA of 9.23 dB are obtained at 2.138 GHz. The measured input and output return losses (S_{11} and S_{22}) characteristics are better than 19 dB. The measured slope of S_{21} is positive over a certain frequency range, which signifies the presence of NGD time. Figs. 8(a) and 11(a) show photographs of the fabricated circuits.

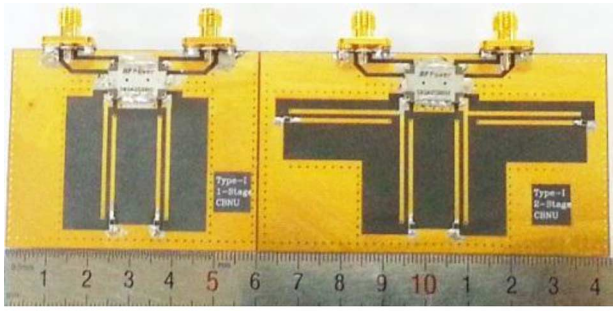

(a) (b)

Fig. 8. Photographs of fabricated circuits of type-I NGD networks. (a) Single-stage and (b) cascaded two-stage.

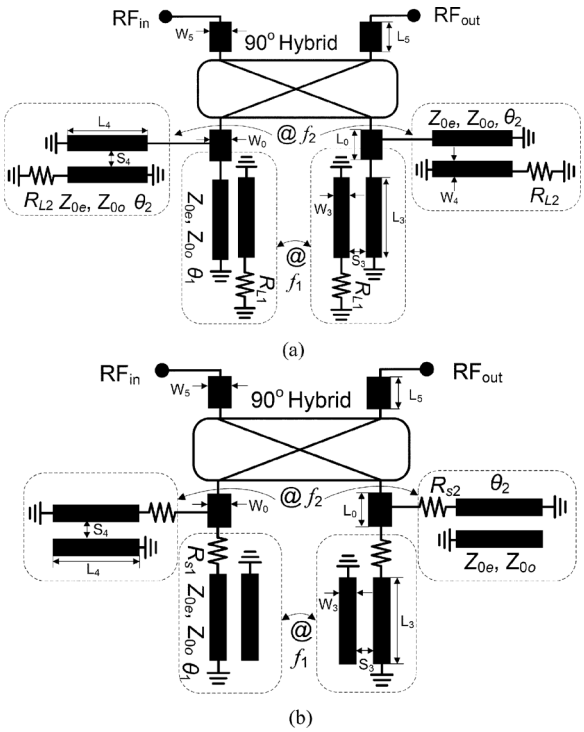

Fig. 9. Structure of cascaded two units of NGD networks with slightly different center frequencies. (a) Type-I and (b) type-II.

TABLE II
PHYSICAL DIMENSIONS OF PARALLEL CONNECTED NGD NETWORKS. (UNITS: MILLIMETERS, REFER TO FIG. 9)

W_0	L_0	W_3	L_3	S_3	R_{L1} (Ω)	R_{S1} (Ω)
2.40	3	1.04	26.25	1.03	3800	105
W_4	L_4	S_4	W_5	L_5	R_{L2} (Ω)	R_{S2} (Ω)
1.04	25.81	1.04	2.40	10	3800	105

B. Parallel Connected NGD Networks for Bandwidth Enhancement

As shown in the previous results of single-stage NGD networks, the NGD bandwidth is small, which is not practically applicable for commercial RF systems. Therefore, it is necessary to enhance the NGD bandwidth. One way to increase the NGD bandwidth is to connect two units of NGD networks operating at different center frequencies in parallel, as shown in Fig. 9. For this purpose, the NGD networks are designed at

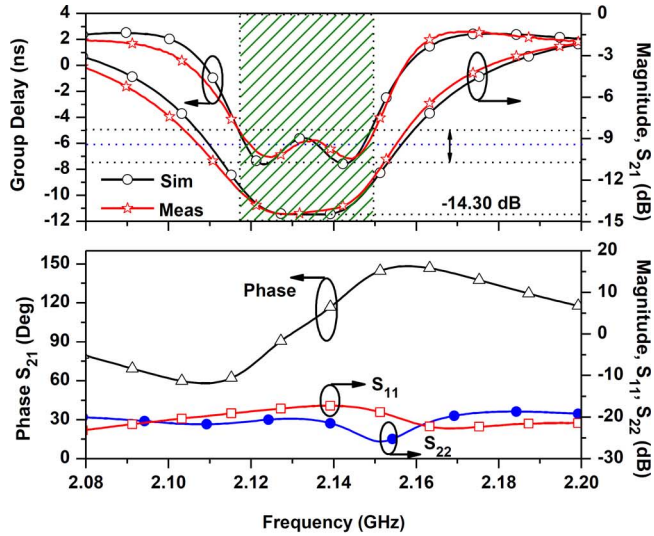

(a)

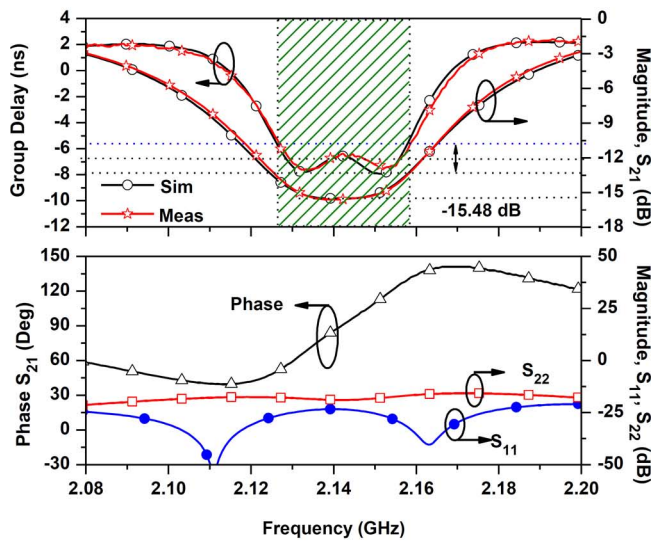

(b)

Fig. 10. Simulation and measurement results of parallel connected two-stage NGD networks for bandwidth enhancement. (a) Type-I and (b) type-II.

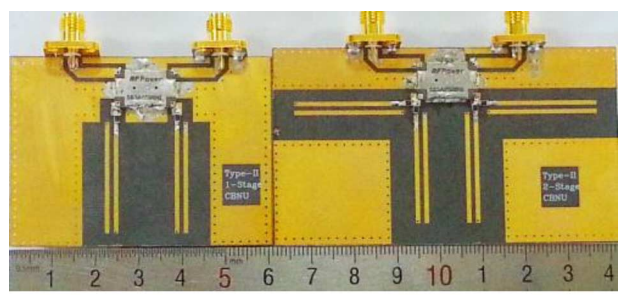

(a) (b)

Fig. 11. Photographs of fabricated circuit of type-II NGD networks. (a) Single-stage and (b) parallel connected two-stage.

TABLE III
PERFORMANCE COMPARISON OF PROPOSED NGD NETWORKS WITH OTHERS WORKS

	f_0 (GHz)	GD_{max} (ns)		S_{21max} (dB)		$GD_{max}\pm$ 1ns BW (MHz)	For R±5% variation	
		A	B	A	B		ΔGD (ns)	ΔS_{21} (dB)
[3]-[4]	2.14	-9.0	-9.0	-33.1	-64.2	35	>46	>23.9
[5]	0.55	-6.0	x	x	x	x	x	x
[13]-[14]	2.14	-8.0	-5.65	-32.8	-62.6	35	>46	>23.9
[15]-[16]	1.0	-10	x	-30	x	x	x	x
[17] *	1.0	-2.0	x	2.0	x	x	x	x
[22]	2.14	-8.9	x	-33	x	25	x	x
[23]-[24]*	0.31	-1.52	x	0.29	x	x	x	x
[26]**	2.14	-6.7	x	-14.3	x	15	<2.2	<2.3
[27]	2.14	-7.9	x	-16.5	x	15	<2.8	<2.9
Type-I	**2.14**	**-7.27**	**-6.40**	**-7.43**	**-14.70**	**32**	**<1.57**	**<1.0**
Type-II	**2.14**	**-6.30**	**-6.85**	**-9.23**	**-15.38**	**33**	**<1.52**	**<0.98**

A = single unit NGD network
B = cascaded two NGD networks
BW = maximum achievable group delay±1ns bandwidth
ΔGD = change in group delay from reference value
ΔS_{21} = change in signal attenuation from reference value
* = gain compensated active NGD networks
** = consists of lumped element parallel (R,L,C) in between transmission lines

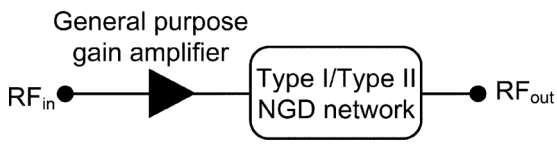

Fig. 12. Block diagram of gain compensated NGD networks.

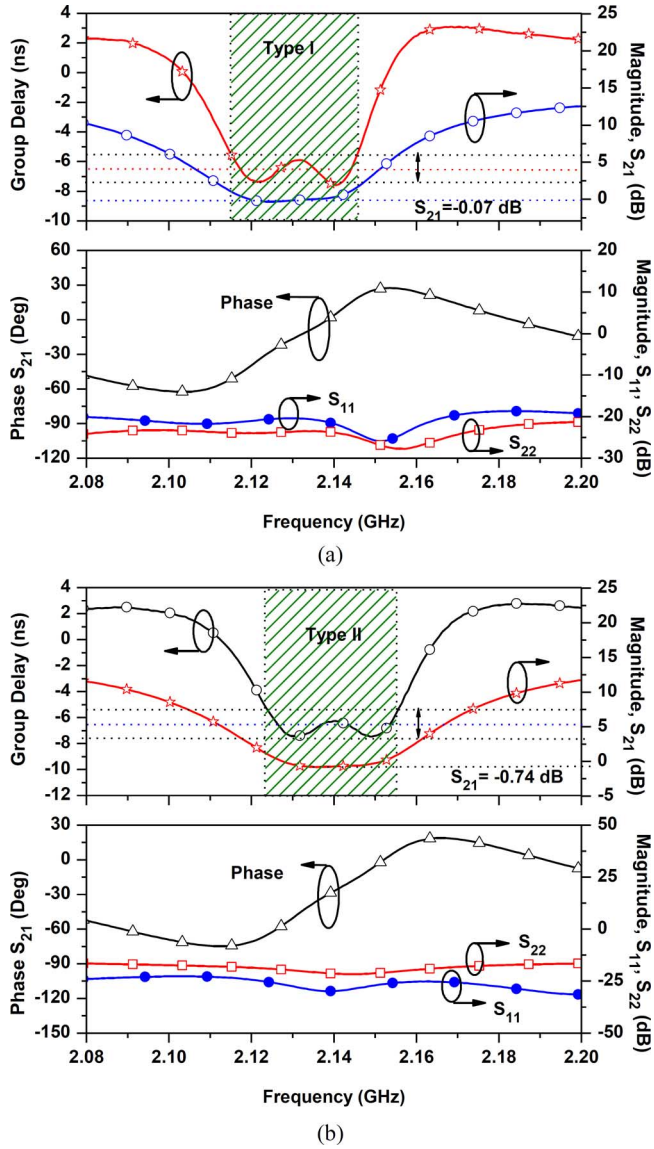

Fig. 13. Measured result of gain compensated NGD networks. (a) Type-I and (b) type-II.

$f_1 = 2.125$ GHz and $f_2 = 2.155$ GHz with predefined GD time of -7 ns. Therefore, the circuit element values of each NGD network are the same as previous, except for the center frequencies. The physical dimensions of these networks are given in Table II.

Fig. 10(a) shows the simulation and measurement characteristics of parallel connected two-stage type-I NGD networks. As shown in this figure, the maximum achievable GD time and SA are obtained as -6.4 ± 0.83 ns and -14.70 dB at 2.135 GHz, which are wider than the single-stage network and shows the practical applicability to the RF system. The measured return-loss characteristics (S_{11} and S_{22}) of this circuit are better than 19 dB. The measured phase slope of S_{21} is positive over a certain region, which signifies the presence of NGD time over that region. Fig. 8(b) shows a photograph of the fabricated type-I NGD network.

Fig. 10(b) shows the simulation and measurement results of parallel connected two-stage type-II NGD networks. The measurement results agree with those of the simulations. From the measurement, the maximum achievable GD time and SA are determined as -6.85 ± 0.83 ns and -15.38 dB at 2.144 GHz. The NGD bandwidth of this circuit is wider than the single-stage network and shows the practical applicability to the RF system. The return loss characteristics (S_{11} and S_{22}) of this circuit are better than 19 dB. The phase slope of S_{21} is positive over a bandwidth of 60 MHz. This positive slope parameter can be used to cancel out the negative phase slope to obtain a zero GD or phase compensation response over a wide bandwidth. Fig. 11(b) shows a photograph of the fabricated type-II NGD network.

Table III shows a performance comparison of the proposed NGD networks from among the previous works. Considering the tradeoff between the achieved NGD time, NGD bandwidth, and SA, the proposed structure provides very low SA compared with previous works. Moreover, the bandwidths of two-stage NGD networks are similar to previous works with the advantage of very low SA. Therefore, the proposed NGD networks are practically applicable to RF systems and reduce the burden of gain amplifiers and can provide stable operations when integrated with RF systems.

C. Gain Compensated NGD Networks

The SA of the proposed NGD networks can easily be compensated with a general-purpose gain amplifier, as shown in Fig. 12. However, it can slightly decrease GD of networks as

well as increase the out-of-band noise. Therefore, the passband SA should be as small as possible in terms of gain compensation and stable operation when NGD networks are integrated into RF systems such as high linear power amplifiers [3], [4], [26]. In this measurement, the general-purpose gain amplifier, ERA-5SM from Mini-Circuits, was used. The measured gain and GD of this general-purpose amplifier are given as 14.63 dB and 0.3 ns, respectively.

Fig. 13 shows the measured results of the SA compensated NGD networks. As seen from measured results, the GD characteristics are almost the same with just only NGD networks, except there are almost no SA at f_0 in case of the SA compensated NGD networks. The maximum achievable GD and SA at f_0 are obtained as -6.1 ± 0.8 ns and -0.07 dB in case of a type-I NGD network and -6.34 ± 0.6 ns and -0.74 dB in case of a type-II NGD network, respectively.

IV. Conclusion

This paper has demonstrated the design and implementation of transmission-line NGD topologies with a predefined GD time and very low SA. The proposed reflective-type NGD networks are based on short-circuited coupled lines. The theoretical analysis shows that very low SA can be obtained because of the high characteristic impedance of coupled lines. To enhance the NGD bandwidth, two NGD networks with slightly different center frequencies are parallel connected, providing wider bandwidth than a single-stage network and demonstrating the practical applicability. The proposed topology can reduce the number of gain compensating amplifier stage and can contribute to the efficiency enhancement as well as out-of-band noise reduction and stable operation when integrated into the power amplifier linearization technique.

References

[1] L. Brillouin and A. Sommerfeld, *Wave Propagation and Group Velocity*. New York, NY, USA: Academic, 1960, pp. 113–137.

[2] M. Kitano, T. Nakanishi, and K. Sugiyama, "Negative group delay and superluminal propagation: An electronic circuit approach," *IEEE J. Sel. Top. Quantum Electron.*, vol. 9, no. 1, pp. 43–51, Jan. 2003.

[3] H. Choi, Y. Jeong, C. D. Kim, and J. S. Kenney, "Efficiency enhancement of feedforward amplifiers by employing a negative group delay circuit," *IEEE Trans. Microw. Theory Techn.*, vol. 58, no. 5, pp. 1116–1125, May 2010.

[4] H. Choi, Y. Jeong, C. D. Kim, and J. S. Kenney, "Bandwidth enhancement of an analog feedback amplifier by employing a negative group delay circuit," *Progr. Electromagn. Res.*, vol. 105, pp. 253–272, 2010.

[5] H. Noto, K. Yamauchi, M. Nakayama, and Y. Isota, "Negative group delay circuit for feed-forward amplifier," in *Proc. IEEE MTT-S Int. Microw. Symp. Dig.*, Jun. 2007, pp. 1103–1106.

[6] B. Ravelo, M. L. Roy, and A. Perennec, "Application of negative group delay active circuits to the design of broadband and constant phase shifters," *Microw. Opt. Technol. Lett.*, vol. 50, no. 12, pp. 3078–3080, Dec. 2008.

[7] S. S. Oh and L. Shafai, "Compensated circuit with characteristics of lossless double negative materials and its application to array antennas," *IET Microw. Antennas, Propag.*, vol. 1, no. 1, pp. 29–38, Feb. 2007.

[8] D. Solli and R. Y. Chiao, "Superluminal effects and negative delays in electronics, and their application," *Phys. Rev. E, Stat. Phys. Plasmas Fluids Relat. Interdiscip. Top.*, no. 5, pp. 056601 1–0566101 4, Nov. 2002.

[9] H. Mirzaei and G. V. Eleftheriades, "Realizing non-Foster reactive elements using negative group delay networks," *IEEE Trans. Microw. Theory Techn.*, vol. 61, no. 12, pp. 4322–4332, Dec. 2013.

[10] S. Kolev, B. Delarcremmonniere, and J. L. Gautier, "Using a negative capacitance to increase the tuning range of a varactor diode in MMIC technology," *IEEE Trans. Microw. Theory Techn.*, vol. 49, no. 12, pp. 2425–2530, Dec. 2001.

[11] Y. Song, S. Lee, E. Cho, J. Lee, and S. Nam, "A CMOS class-E power amplifier with voltage stress relief and enhanced efficiency," *IEEE Trans. Microw. Theory Techn.*, vol. 58, no. 2, pp. 310–317, Feb. 2010.

[12] D. J. Gregoire, C. R. White, and J. S. Colburn, "Wideband artificial magnetic conductors loaded with non-Foster negative inductors," *IEEE Antennas Wireless Propag. Lett.*, vol. 10, pp. 1586–1589, 2011.

[13] Y. Jeong, H. Choi, and C. D. Kim, "Experimental verification for time advancement of negative group delay in RF electronics circuits," *Electron. Lett.*, vol. 46, no. 4, pp. 306–307, Feb. 2010.

[14] H. Choi, Y. Kim, Y. Jeong, and C. D. Kim, "Synthesis of reflection type negative group delay circuit using transmission line resonator," in *Proc. 39th Eur. Microw. Conf.*, Sep. 2009, pp. 902–605.

[15] S. Lucyszyn, I. D. Robertson, and A. H. Aghvami, "Negative group delay synthesizer," *Electron. Lett.*, vol. 29, no. 9, pp. 798–800, Apr. 1993.

[16] S. Lucyszyn and I. D. Robertson, "Analog reflection topology building blocks for adaptive microwave signal processing applications," *IEEE Trans. Microw. Theory Techn.*, vol. 43, no. 3, pp. 601–611, Mar. 1995.

[17] B. Ravelo, A. Perennec, M. L. Roy, and Y. G. Boucher, "Active microwave circuit with negative group delay," *IEEE Microw. Wireless Compon. Lett.*, vol. 17, no. 12, pp. 861–863, Dec. 2007.

[18] H. Choi, K. Song, C. D. Kim, and Y. Jeong, "Synthesis of negative group delay time circuit," in *Proc. Asia–Pacific Microw. Conf.*, 2008, pp. 1–4.

[19] C. D. Broomfield and J. K. A. Everard, "Broadband negative group delay networks for compensation of microwave oscillators and filters," *Electron. Lett.*, vol. 9, no. 23, pp. 1931–1932, Nov. 2000.

[20] B. Ravelo, A. Perennec, and M. L. Roy, "Synthesis of broadband negative group delay active circuits," in *IEEE MTT-S Int. Microw. Symp. Dig.*, Jun. 2007, pp. 2177–2180.

[21] G. Chaudhary, Y. Jeong, and J. Lim, "Microstrip line negative group delay filters for microwave circuits," *IEEE Trans. Microw. Theory Techn.*, vol. 62, no. 2, pp. 234–243, Feb. 2014.

[22] H. Choi, Y. Kim, Y. Jeong, and J. Lim, "A design of size-reduced negative group delay circuit using a stepped impedance resonator," in *Proc. Asia–Pacific Microw. Conf.*, Dec. 2010, pp. 118–1121.

[23] M. Kandic and G. E. Bridges, "Bilateral gain-compensated negative group delay circuit," *IEEE Microw. Wireless Compon. Lett.*, vol. 21, no. 6, pp. 308–310, Jun. 2011.

[24] M. Kandic and G. E. Bridges, "Asymptotic limit of negative group delay in active resonator-based distributed circuits," *IEEE Trans. Circuits Syst. I, Reg. Papers*, vol. 58, no. 8, pp. 1727–1735, Aug. 2011.

[25] O. F. Sidhiqui, M. Mojahedi, and G. V. Eleftheriades, "Periodically loaded transmission line with effective negative group delay index and negative group velocity," *IEEE Trans. Antennas Propag.*, vol. 51, no. 10, pp. 2619–2625, Oct. 2010.

[26] H. Choi, G. Chaudhary, T. Moon, Y. Jeong, J. Lim, and C. D. Kim, "A design of composite negative group delay circuit with lower signal attenuation for performance improvement of power amplifier linearization techniques," in *IEEE MTT-S Int. Microw. Symp. Dig.*, Jun. 2011, pp. 1–4.

[27] G. Chaudhary and Y. Jeong, "Distributed transmission line negative group delay circuit with improved signal attenuation," *IEEE Microw. Wireless Compon. Lett.*, vol. 24, no. 1, pp. 20–22, Jan. 2014.

[28] G. Chaudhary and Y. Jeong, "Transmission line negative group delay networks with improved signal attenuation," *IEEE Antennas Wireless Propag. Lett.*, vol. 13, pp. 1039–1042, 2014.

[29] P. Phudpong and I. C. Hunter, "Frequency selective limiters using nonlinear bandstop filters," *IEEE Trans. Microw. Theory Techn.*, vol. 57, no. 1, pp. 157–164, Jan. 2009.

[30] I. C. Hunter, J. D. Rhodes, and V. Dassonvile, "Triple mode dielectric resonator hybrid reflection filters," *Proc. Int. Elect. Eng.– Microw. Antennas Propag.*, vol. 145, no. 4, pp. 337–343, Aug. 1998.

[31] I. C. Hunter, *Theory and Design of Microwave Filters*, ser. Electromagn. Wave. Stevenage, U.K.: IET, 2001.

[32] H. R. Ahn and B. Kim, "Small wideband coupled-line ring hybrids with no restriction on coupling power," *IEEE Trans. Microw. Theory Techn.*, vol. 57, no. 7, pp. 1806–1817, Jul. 2009.

[33] H. R. Ahn and S. Nam, "Wideband coupled-line microstrip filters with high-impedance short-circuited stubs," *IEEE Microw. Wireless Compon. Lett.*, vol. 21, no. 11, pp. 586–588, Nov. 2011.

Girdhari Chaudhary (S'10–M'13) received the B.E. degree in electronics and communication engineering from the Nepal Engineering College (NEC), Kathmandu, Nepal, in 2004, the M.Tech. degree in electronics and communication engineering from the Malaviya National Institute of Technology (MNIT), Jaipur, India, in 2007, and the Ph.D. degree in electronics engineering from Chonbuk National University, Jollabuk-do, Korea, in 2013.

He is currently a Post-doctoral Researcher with the HOPE-IT Human Resource Development Center-BK21 PLUS, Division of Electronics Engineering, Chonbuk National University. He has authored or coauthored over 30 papers in international journals and conference proceedings. His research interests include multi-band tunable passive circuits, NGD circuits and their applications, and high-efficiency power amplifiers.

Yongchae Jeong (M'99–SM'10) received the B.S.E.E., M.S.E.E., and Ph.D. degrees in electronics engineering from Sogang University, Seoul, Korea, in 1989, 1991, and 1996, respectively.

From 1991 to 1998, he was a Senior Engineer with Samsung Electronics. From 1998, he joined the Division of Electronics Engineering, Chonbuk National University, Jollabuk-do, Korea. From July 2006 to December 2007, he was with the Georgia Institute of Technology, as a Visiting Professor. He is currently a Professor and member of the Information Technology (IT) Convergence Research Center, and Director of the HOPE-IT Human Resource Development Center, BK21 PLUS, Chonbuk National University. He currently teaches and conducts research in the area of microwave passive and active circuits, mobile and satellite base-station RF systems, design of periodic defected transmission lines, and RF integrated circuit (RFIC) design. He has authored or coauthored over 100 papers in international journals and conference proceedings.

Dr. Jeong is a member of the Korea Institute of Electromagnetic Engineering and Science (KIEES).